RARE METALS
Vol. 31, No. 1, Feb. 2012, p. 81
DOI: 10.1007/s12598-012-0467-x

Characterizations and mechanical properties of impregnated diamond segment using Cu-Fe-Co metal matrix

LI Wensheng[a], ZHANG Jie[a], WANG Shucai[b], DONG Hongfeng[a], LI Yaming[a], and LIU Yi[a]

[a] *State Key Laboratory of Advanced Non-Ferrous Materials, Lanzhou University of Technology, Lanzhou 730050, China*
[b] *National Center for Advanced Tribology, School of Engineering Sciences, University of Southampton, Southampton, SO17 1BJ, UK*

Received 10 June 2011; received in revised form 30 June 2011; accepted 11 July 2011

Abstract

Diamond impregnated Cu-Fe-Co based saw-blade segments are directly processed by vacuum and pressure-assisted sintering at different temperature, with the purpose of reducing the cobalt content in diamond tools. Copper and iron are used as the bonding elements and cobalt-chrome pre-alloyed powder is used as the hardening phase. Effects of sintering temperature on microstructures and mechanical properties of the sintered matrix and diamond graphitization were investigated by X-ray diffraction analysis, electron probe micro-analyzer, universal testing machine, digital Rockwell hardness tester and Raman scattering analyzer. Results showed that microstructures of the sintered matrix were refined and porosities in the sintered matrix were closed to a more spherical-like shape with the increase of the sintering temperature. Densification, hardness and tensile strength of the matrix sintered at 820 °C were 12.75%, 2.72% and 156.38% higher than that of the matrix sintered at 740 °C, respectively. Diamond graphitization was not occurred at 820 °C. The hardness and the tensile strength rose 32.8% and 13.5%, respectively, after 7.5 h ageing treatment. The matrix densification ascent and the dispersed distribution of Co-Cr pre-alloyed powders contributed a hardness improvement and a tensile strength improvement to the Cu-Fe based matrix.

Keywords: Cu-Fe-Co based matrix; sintering temperature; graphitization; microstructure; mechanical properties

1 Introduction

Diamond saw-blades are widely used for sawing, cutting, grinding and trimming stone, concrete and tiles. These tools consist of two main elements, the steel core and the segments (Fig. 1), the latter being joined to the steel core by brazing or laser-welding. The diamonds from microns to tens of microns are sintered with other metal matrix according to the usage of the saw-blades. The geometry of the diamond saw blade and the force distribution in a diamond particle in matrix are illustrated in Fig. 1. The compressive stress arises from the different thermal expansion coefficient between diamond and matrix. Yield strength and hardness of the matrix are two of the key facts that related to retention of the fixed diamond, which was determined by the friction/adhesion between the diamond grits and the matrix [1]. Thus, the effect of diamonds in tools depends upon the preparation process and matrix materials that are used to hold and support the diamonds during cutting [1–2].

Nowadays, impregnated diamond segments are fabricated by hot pressing and metal infiltration on a large scale, with a minority processed by cold pressing and sintering. During the processing, the diamond particles are bonded to the metal matrix by means of a combination of chemical reaction and physical interactions. However, the sintering process and parameters must be controlled carefully to avoid attack, dissolution and/or graphitization of the diamonds, which negatively affects the final cutting performance of the tools. The bonds obtained at low temperatures (less than 850 °C) preserve diamond crystal properties best [3].

The metal materials acting as the bonding matrix in the impregnated diamond composite depend strongly on the abrasiveness and hardness [4]. Normally tungsten is used as a diamond bonding matrix for cutting materials such as concrete and some granites, W–Co and Co alloys are used to cut granites in general, and Co, Co–bronze and Fe–Co with the cobalt content from 18 wt.%~25 wt.% are widely used in diamond impregnated tools for cutting marbles [5–8]. Cobalt has good chemical compatibility with diamond at the processing temperatures and excellent diamond retention associated with a satisfactory wear resistance after some cutting operations.

Corresponding author: ZHANG Jie **E-mail:** zj_lanzhou@126.com

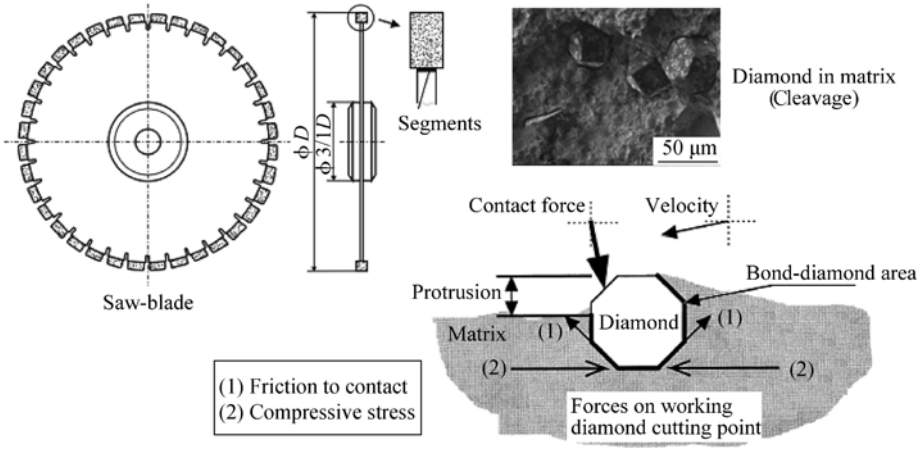

Fig. 1 Saw-blade tools for stone cutting and the forces on working diamond

Nevertheless, the cobalt is a strategic metal, and its trade price is subject to great value, so cobalt is no longer the best choice in some diamond tools' applications. Considering all these negative points, researchers have recently developed or proposed new alloys that may be used as metal matrix in diamond tools, aiming at the minimization of the Co content—exemplified by the Fe-Cu-Co alloys seen in Refs. [9–10].

This paper is dedicated to the study of a novel Cu-Fe-Co system (with cobalt addition less than 5.0 wt.%) as bonding metallic matrix for use in impregnated diamond tools [11], aiming to process diamond segments with the same performance as the commercial saw-blade segments for marble cutting.

2 Experimental

2.1 Specimen preparation

Table 1 shows the composition of Cu-Fe-Co based matrix of the sintered diamond segments. Copper and nickel are electrolytic powders with the purity of 99.7% and the sizes from 75 to 100 μm. Fe is high-grade reduced iron powder with the purity of 99.7% and the size from 75 to 100 μm. Cobalt is supplied by gas atomized Co-Cr pre-alloy powders with a composition of 75% Co and 25% Cr, and the sizes from 80 to 125 μm, which had a Cr content of 25 wt.% and balanced by Co. The diamond grits are the MBD_{12} type synthetic diamond with the sizes from 270 to 380 μm.

Table 1 Composition of Cu-Fe-Co based matrix

Ingredients (Powders mixed)	Content / wt.%
Cu	45~55
Fe	34~38
Ni	5~10
Co-Cr pre-alloyed powder	5~8
Sn	1~3

Metallic powders were weighed according to the matrix composition, and 0.7 wt.% industry ethanol acting as a forming agent was added, which aims at avoiding the segregation between diamond grits and metallic powders because of the diffidence of sizes and density. Then, the whole mixture were put into the 2000 cm^3 mixing-tank of a three-dimensional vortex mixer (TD-2) and mixed for 1 h at the speed of 24 $r \cdot min^{-1}$.

Then the mixture was weighed and loaded into the graphite mould, which has different sizes according to the experimental standard or the in situ industry requirement. The loaded graphite moulds were sintered in a vacuum and pressure-assisted sintering machine (RYJ-2000Z) at 740, 780 and 820 °C under the pressure of 13 MPa, the heating rate is about 100~150 $°C \cdot min^{-1}$, the holding time at the sintering temperature is 3 min. The samples were cooled down in the furnace to 450 °C at a cooling rate of 180~200 $°C \cdot min^{-1}$, then were taken out to air cooling, and ageing treatment at 500 °C for 7.5 h was performed.

2.2 Microstructure and graphitization analyses

The specimens for metallographic examination were prepared using standard polishing techniques and etched by the solution consisting of 5 g $FeCl_3$, 10 ml HCl and 100 ml distilled water. Scanning electron microscopy (SEM-6700F) with energy dispersive spectroscopy (EDS) were used to examine the microstructures of the specimens. Electron probe micro-analyzer (EPMA-1600) fitted with wave dispersion X-ray spectroscopy (WDS) was employed for micro-constituents analysis. X-ray diffraction (Germany broker D8 ADVANCE XRD) was used for phase analysis, with a copper target (Cu-Kα radiation, $\lambda = 0.154$ nm). Raman spectrometer (in Via-Reflex) with the resolution of 0.15 cm^{-1} was used to test the graphitization tendency of the diamond grits.

2.3 Densification and mechanical tests

The bulk density ρ_b of the sintered samples was tested according to the Archimedes law, using a digital balance (CP225D) with an error within 0.01 mg and a graduated cylinder with the resolution of 0.5 ml.

The densification was calculated according to Eq. (1):

$$\rho_{re} = \frac{\rho_b}{\rho_{th}} \times 100\% \quad (1)$$

where ρ_{re} is the relative theoretical density, also called densification in powder metallurgy. ρ_{th} is the theoretical density.

Rockwell B hardness was tested on a digital Rockwell hardness tester (MODEL HRC-150) with a load of 1839 N. The micro-hardness was tested on the HD1-187.5 Sclero-meter by Vickers with a load of 4.9 N. Tensile strength tests were performed on a universal testing machine (AG-10TA) at a loading rate of 1 mm·min^{-1}. The diameter of the tensile specimens were 10 mm according to ASTM E 8M. Four samples were tested.

3 Results

3.1 Microstructures

Fig. 2 (a~c) show the backscattered electron images of the Cu-Fe-Co based matrixes without diamond added, which were sintered at 740 °C (SS), 780 °C (SS) and 820 °C (SS), respectively. The numbers of the dark pores in the sintered matrix were reduced and the shape of the dark pores varied from irregular to round with the increase of the sintering temperature, as shown by the arrows in the Fig. 2 (a~c). The dark phase was well distributed in Fig. 2 (c) compared to that in Fig. 2 (a). Fig. 2 (d~f) are the backscattered electron images of the samples that were aged and are designated as 740 °C (AS), 780 °C (AS) and 820 °C (AS). There are less white phase in the AS samples than that in the SS samples.

Fig. 3 shows the X-ray diffraction patterns of the sintered matrixes at 740, 780 and 820 °C. The diffraction peaks are quite similar. Combined with the composition, three phases have been identified: a-Cu (fcc); b-Fe (bcc) and c-Co (fcc). It is interesting that two peaks related to Co (2θ=51.88° and 7635°, respectively) decrease with the increase of the sintering temperature.

Fig. 4 is the high-resolution backscattered electron image of the sample sintered at 820 °C. Micro-constituents semi-quantitatively analysis and phase compositions definitions were done using WDS attached in EPMA. It shows that the grey round phase, which is pointed by Character A in Fig. 4, is the Co-Cr pre-alloy powder with a chemical composition of approximately 55.8 wt.%Co, 28.0 wt.%Cr, etc. The dark grey and grey continuous phases, which are pointed by Characters B and C, are the Fe enriched matrix phase and the Cu enriched matrix phase, with the chemical compositions of approximately 90.9 wt.%Fe, 9.0 wt.%Ni, etc. in the dark grey B phase and 94.9 wt.%Cu, 5.0 wt.%Sn, etc. in the grey C phase, respectively. The white phase, which is pointed by Character D, is the Sn enriched phase with a chemical composition of approximately 42.8 wt.%Cu, 30.1 wt.%Ni and 27.1 wt.%Sn. The composition of the Sn enriched phase D reveals that the Cu-Sn and Ni-Sn low melting-point compounds are formed during the sintering, although it is not detected by the X-ray diffraction.

Fig. 5 (a) is the SEM morphology of the polished segment that is sintered at 820 °C. The diamond grits are well distributed and the cubic-octahedral shape of diamond is clear after the sample was grinded and polished. Fig. 5 (b) is the SEM morphology of the broken cross-section of the segment that is sintered at 820 °C. Diamond cleavage that caused during the breaking would be found. Raman spectra analysis was performed on the embedded diamond grit in the breaking section; it reveals that there is only the sharp

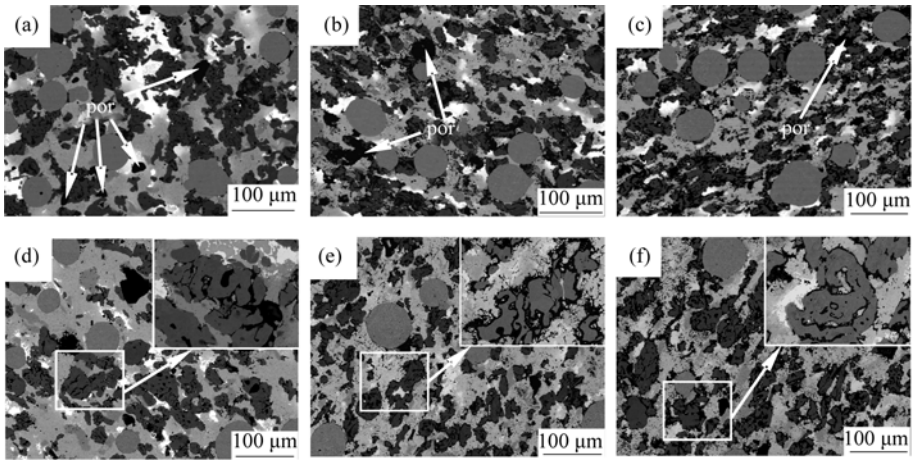

Fig. 2 Backscattered electron images of matrix samples
(a) 740 °C SS; (b) 780 °C SS; (c) 820 °C SS; (d) 740 °C AS; (e) 780 °C AS; (f) 820 °C AS

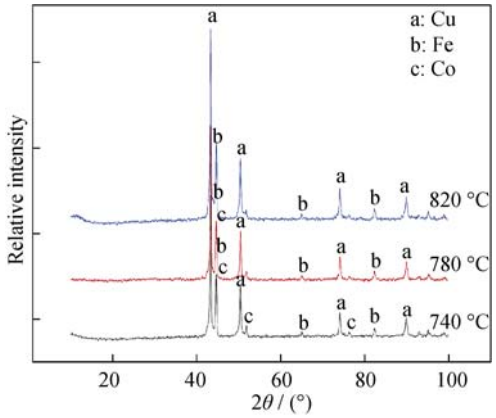

Fig. 3 XRD patterns of matrix samples sintered at different temperatures

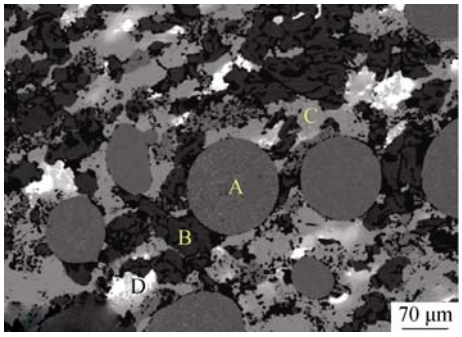

Fig. 4 High-resolution backscattered electron image of the matrix sintered at 820 °C

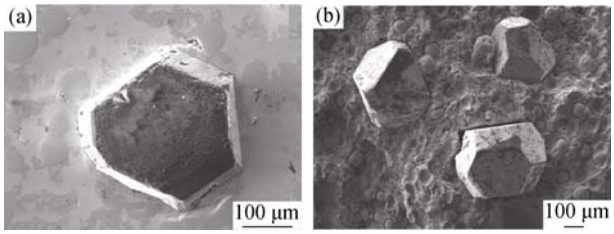

Fig. 5 Second electron images of the segment sintered at 820 °C (a) Polished segment surface; (b) Broken segment cross-section

scattering peak from diamond at around 1333 cm^{-1} [12]. The graphite peak at around 1581 cm^{-1} is not detected as shown in Fig. 6. These results suggest that the diamond of the sample sintered at 820 °C is not graphitized during the sintering.

3.2 Densification and mechanical properties

Table 2 shows the densification of the matrix samples sintered at different temperatures. It was found that the densification increased with sintering temperature. The densification of the sample sintered at 780 °C is 4.03% higher than that of the sample sintered at 740 °C, and the densification of the sample sintered at 820 °C is the highest among these three, which achieved to 99.02% of the theoretical

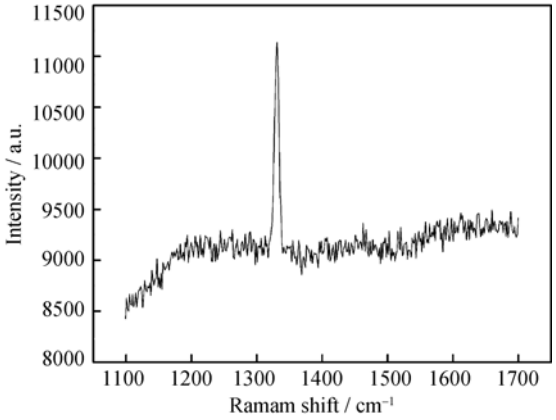

Fig. 6 Raman scattering spectrum on diamond of the segment sintered at 820 °C

Table 2 Densification of the sintered samples

Samples	Sintering temperature / °C	Densification / %
A	740	87.82
B	780	91.36
C	820	99.02

density, and is 12.75% higher than that of the sample sintered at 740 °C.

Fig. 7 is Rockwell B hardness of the SS and AS samples at different temperatures. It shows that hardness of the sintered samples is increased with sintering temperature. Hardness of the sample sintered at 780 °C is 2.24% higher than that of the sample sintered at 740 °C, and hardness of the sample sintered at 820 °C is the highest among these three and goes up to 99.467 HRB, which is 2.72% higher than that of the sample sintered at 740 °C. The hardness of the AS samples averagely rose 32.80% after 7.5 h ageing treatment. The microhardness test on the sample sintered at 820 °C shows that the microhardness of the grey round phase A in Fig.5 was 466.2 HV; the microhardness of matrix phases, i.e. phase C, B, D in Fig. 5 is around 92.7 HV.

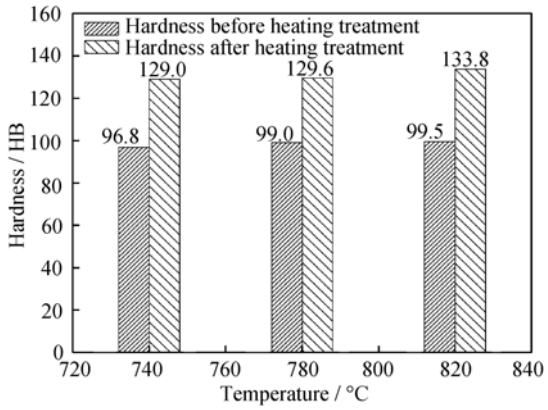

Fig. 7 Hardness of samples sintered and aged at different temperatures

Evidently, the round phase is hardest in the sintered matrix and can be a strengthening particle to the sintered matrix.

Fig. 8 is the tensile strength of the SS and AS samples at different temperatures. It revealed that the tensile strength of the samples was increased with sintering temperature. The tensile strength of the sample sintered at 820 °C reached to 252.30 MPa and was 156.38% higher than that of the sample sintered at 740 °C. Age treatment averagely raised the tensile strength of the samples 13.5%.

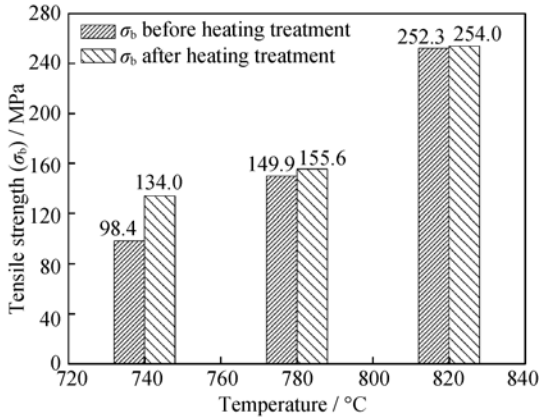

Fig. 8 Tensile strength of samples sintered and aged at different temperatures

4 Discussion

4.1 Relationships between microstructure and sintering temperature

As it was shown in Table 2, the densification of the sintered matrix samples was increased with sintering temperature. Firstly, under a pressure of 13 MPa, the higher the sintering temperature is, the more mutual solubility among the metal powders will be enhanced. The low melting point metals such as Sn and Cu powders surface will be molten and tend to form a large amount of liquid phase, which reduces the friction between the powder particles, and thus the pore closure occurred [6]. Ageing is an effective way to enhance diffusion and solution. There are less white phases after ageing treatment which were rich in Sn, as shown in Fig. 2 (d~f). Secondly, the higher the sintering temperature is, the further plastic flow among the high strain deformed powder particles will be improved, which results in a high dense in the pressure-assisted sintering [1]. With the sintering temperature increase, the number of the pores in the sintered matrix was reduced, and the shape of the pores in the sintered matrix became more spherical-like, which contribute the matrix a low unfilled volume and a high densification. The densification of the sample sintered at 820 °C is achieved to 99.02% of the theoretical density.

The dark grey phases in Fig. 2 (b,c), which are Fe enriched high melting point phase as has been proved by WDS analysis in Fig. 4, are smaller and more uniformly distributed than in Fig. 2 (a). The higher the sintering temperature is, the further does the microstructure be refined.

To the diamond, it has been proved by the Raman spectra analysis that no graphitization occurred. Diamond is a metastable allotrope of carbon even under the conditions such as low temperature. The graphitization of diamond is related to sintering temperature, sintering atmosphere, the purity of diamond powders and so on. The structure of diamond remains stable only due to a kinetic difficulty in rebuilding of the lattice at the sintering temperature of 820 °C [7, 12]. On the other hand, the sintering was processed in vacuum; no oxygen can react with diamond to produce CO or CO_2 that results in accelerating graphitization [12].

4.2 Relationships between mechanical properties and microstructure

Fig. 7 reveals that hardness of the sintered matrix was increased with sintering temperature. Hardness of the sample sintered at 820 °C was the highest and went up to 99.467 HRB, which is 2.72% higher than that of sample sintered at 740 °C. Hardness of the metallic matrix is one of the vital factors which determine tool life and cutting efficiency, for the reason that the metallic bonder must be worn out at just the optimum rate to keep the diamonds being exposed for maximum cutting efficiency [4]. The first fact is the solid solutions, such as Fe-Ni, Cu-Sn and Cu-Ni, increased with the increase of the sintering temperature. After ageing treatment, the dark phases inside the gray phases are more dispersive, as the high magnified rectangular areas at the up-right corner in Figs. 2 (d~f) showed. The second fact is the matrix's densification that became tighter and the porosities that were further excluded inside the sintered matrix with the increase of the sintering temperature, as Figs.2 (a~c) showed.

Fig. 8 reveals that the tensile strength of the sintered matrix was increased with sintering temperature. The σ_b of the sample sintered at 820 °C was the highest and reached to 252.30 MPa, and was 156.38% higher than that of the sample sintered at 740 °C. Tensile strength of the sintered matrix is influenced by the matrix's microstructure. Firstly, it can be attributed to the solid solution which occurs more effectively at higher sintering temperature, although in small amounts and not being read by XRD [1, 7, 13]. The tensile strength averagely raised 13.5% by age treatment. Secondly, it is due to the grain refining strengthening according to the Hall-Petch relationship [14] as showed in Eq. (2).

$$\sigma_s = \sigma_o + Kd^{-\frac{1}{2}} \tag{2}$$

where σ_s is the tensile yield strength, σ_0 is the Peierls stress,

Table 3 Results of densification, hardness, wear resistance and yield strength of Cu-Fe-Co alloys

Material	Densification / %	Rockwell B hardness / HRB	Wear resistance, WR / %	Tensile strength / MPa	References
Cu-Fe-Co based alloy[1]	99.2	99.467	1.928 - 2.012	252.292	This work
NEXT 100[2]	76.64±0.77	118.9±0.2	2.096±0.055	-	[8]
NEXT 200[3]	97.0	107.0	-	-	[1]
Fe-60Cu-20Co[4]	78.9	125.8±0.7	1.700.01	-	[6]
Fe-20Cu-1SiC[5]	-	39 HB	0.54	88±5	[7]

1: Mixed powders, vacuum pressure-assisted sintering at 13 MPa/820 °C/3 min/1 Pa vacuum
2: Pre-alloyed Cu-25 wt.%Fe-25 wt.%Co powder, hot pressed at 35 MPa/600-750 °C/3 min
3: Pre-alloyed Cu-14.7 wt.%Fe-22.6 wt.%Co powder , hot pressed at 35 MPa/800 °C/3 min
4: Mixed powders, pressureless sintering at 1150 °C/25 min/1 Pa vacuum
5: Mixed powders, pressureless sintering at 1150 °C/25 min/1.3 Pa vacuum

K denotes the strength of the cell boundaries, d is the grain size.

It is found that the σ_s values increase with the decreasing of the d values according to the Hall-Petch relationship. The grain size in the sintered matrix was refined with the increase of the sintering temperature, as shown in Fig. 2, which contributes the matrix sintered at higher temperature higher tensile yield strength.

Thirdly, it is also due to the second phase dispersion strengthening, which was described by G.S. Ansell and F.V. Lenel [15]in Eq. (3).

$$\tau_c = \sqrt{\frac{GbG^*}{2\lambda C}} \tag{3}$$

where τ_c is shear yield stress, G is shear modulus of metal matrix, b is burgers vector, G^* is shear modulus of second solid particles, λ is distance between dispersed particles, C is a constant.

It is found that the τ_c values increase with the decreasing of the λ values according to Eq. (3). The grain size and microstructure in the sintered matrix were refined with the increase of the sintering temperature, as shown in Fig. 2, which results in a small distance between two Co-Cr hard particles that existed as hard particles in the sintered matrix. As point A in Fig. 4, the Co-Cr pre-alloyed powders seem to not be affected by the sintering temperature. There would be some solid diffusion but no liquid phase appears on their surface. There is a smaller distance between the dispersed hard particles, which contributes the matrix sintered at high temperature higher compressive yield strength.

4.3 Comparisons with the other works

Table 3 presents the results of densification, hardness, wear resistance and tensile strength of 5 types of Cu-Fe-Co alloys matrix for diamond tools which were prepared by different ways. It can be seen that the densification values of this work are similar to the results in Ref. [1], and are quite superior to those of any other works. The hardness values in this work are a little bit lower than those in other works, but the tensile strength seems higher a lot than that of the pressureless sintered Fe-20Cu-1SiC alloy. Nearly the same cutting performance and ability can be achieved. In situ application of the diamond segments produced in this work proved that the tools have the same cutting performance to the products in other works, and the low Co content returns in a low materials cost.

5 Conclusions

(1) Microstructure of Cu-Fe-Co based sintered segment matrix is very sensitive to the sintering temperature. Pore closure and densification increase contribute the sintered matrix with high tensile strength.

(2) Diamond graphitization does not occur at the sintering temperature of 820 °C.

(3) The high hardness Co-Cr pre-alloyed powders hardened Cu-Fe based sintered matrix.

(4) In situ application of the Cu-Fe-Co based diamond segments proved that Cu–Fe-Co based matrix bonds may probably be used in diamond segments for marble cutting, and a low materials cost in return because of the low Co content.

Acknowledgments

The project was financially supported by Gansu Key Technology Project (No. 090JKCA050) and Gansu Outstanding Youth Foundation (No. 201105).

References

[1] Viliar M., Muro P., Sanchez J.M., Iturriza I. and Castro F., Consolidation of diamond tools using Cu-Co-Fe based alloys as metallic binders, *Powder Metallurgy*, 2001, **44** (1): 82.

[2] Ilio A.D., and Togna A., A theoretical wear model for dia-

mond tools in stone cutting, *International Journal of Machine Tools and Manufacture*, 2003, **43** (11): 1171.

[3] Zeren M., and Kargoz S., Sintering of polycrystalline diamond cutting tools, *Materials & Design*, 2007, **28** (3): 1055.

[4] Webb S.W., Diamond retention in sintered cobalt bonds for stone cutting and drilling, *Diamond and Related Materials*, 1999, **8** (11): 2043.

[5] Silva S., Mammana V.P., Salvadori M.C., Monteiro O.R. and Brown I.G., WC-Co cutting tool inserts with diamond coatings, *Diamond and Related Materials*, 1999, **8** (9): 1913.

[6] Barbosa A.P., Bobrovnitchii G.S., Skyry A.L., Guimars RS. and Filgueira M., Structure, microstructure and mechanical properties of PM Fe–Cu–Co alloys, *Material and Design*, 2010, **31** (1): 522.

[7] Oliveriar L., Bobrovnitchii G.S., and Figuleira M., Processing and characterization of impregnated diamond cutting tools using a ferrous metal matrix, *International Journal of Refractory Metals and Hard Materials*, 2007, **25** (4): 328.

[8] Oliverira H.C., Cabral S.C., Cuimaraes R.S., Bobrovnitchii G.S., and Filgueira M., Processing and characterization of a cobalt based alloy for use in diamond cutting tools, *Materials Science and Engineering Technology*, 2009, **40** (12): 907.

[9] Clark I.E., and Kamphuis B.J., Cobalite HDR-a new prealloyed matrix powder for diamond construction tools, *Industrial Diamond Review*, 2002, **62** (3): 177.

[10] Weber G., and Weiss C., DIAMIX: A family of bonds based on DIABASE-V21, *Industrial Diamond Review*, 2005, **65** (2): 28.

[11] Li W.S., Yuan K.X., Li G.Q., and Lu Y., Investigation on Cu-Fe based diamond composite preparation and properties, *Materials Review*, 2010, **24** (1): 78.

[12] Solin S.A., and Ramadas A.K., Raman spectrum of diamond, *Physical Review B*, 1970, **1** (4): 1687.

[13] Thorat R.R., Brahmankar P.K., and Mohan T.R.R., Consolidation behavior of Cu-Co-Fe pre-alloyed powders, [in] *International Symposium of Research Students on Material Science and Engineering, Chennai: Indian Institute of Technology Madras*, 2004: 1.

[14] Go Y.S., and Spitzig W.A., Strengthening in deformation-processed Cu-20%Fe composites, *Journal of Materials Science*, 1991, **26** (1): 163.

[15] Ansell G.S., and Lenel F.V., Criteria for yielding of dispersion-strengthened alloys, *Acta Metallurgica*, 1960, **8** (9): 612.